Supplementary Information

Rationally Designed Freestanding Peapod-like Carbon-coated V_2O_3 Nanowires Film Cathodes Enable Highly Stable Aqueous Zinc-ion batteries

Xingxing Li,[a]* Linling Zheng,[a] Zhirui Huang,[a] Meichen Ding,[a] Haishu Wu,[a] Hao Xie,[a] Mengying Xu,[a] Guoqiang Ma,[b] and Biao Gao [c]*

[a]School of Materials Science and Energy Engineering, Hubei University of Education, Wuhan 430205, China

E-mail: lixingxing@hue.edu.cn

[b]School of Applied Physics and Materials, Wuyi University, Jiangmen 529020, China

[c]The State Key Laboratory of Refractories and Metallurgy and Institute of Advanced Materials and Nanotechnology, Wuhan University of Science and Technology, Wuhan 430081, China

Corresponding authors:

E-mail: lixingxing@hue.edu.cn

E-mail: gaobiao@wust.edu.cn

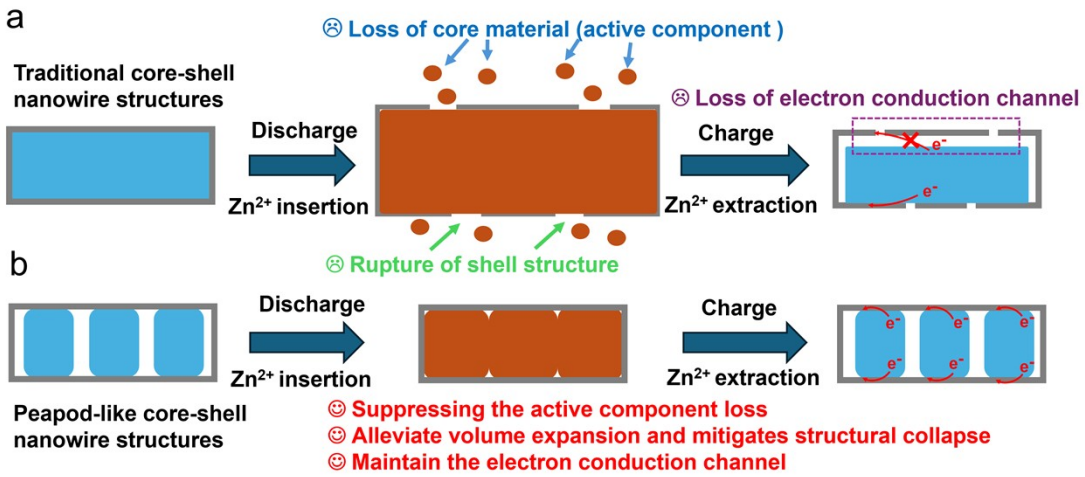

Fig. S1. Schematic illustration of the dynamics and stability in traditional core-shell nanowire structures and peapod-like core-shell nanowire structures.

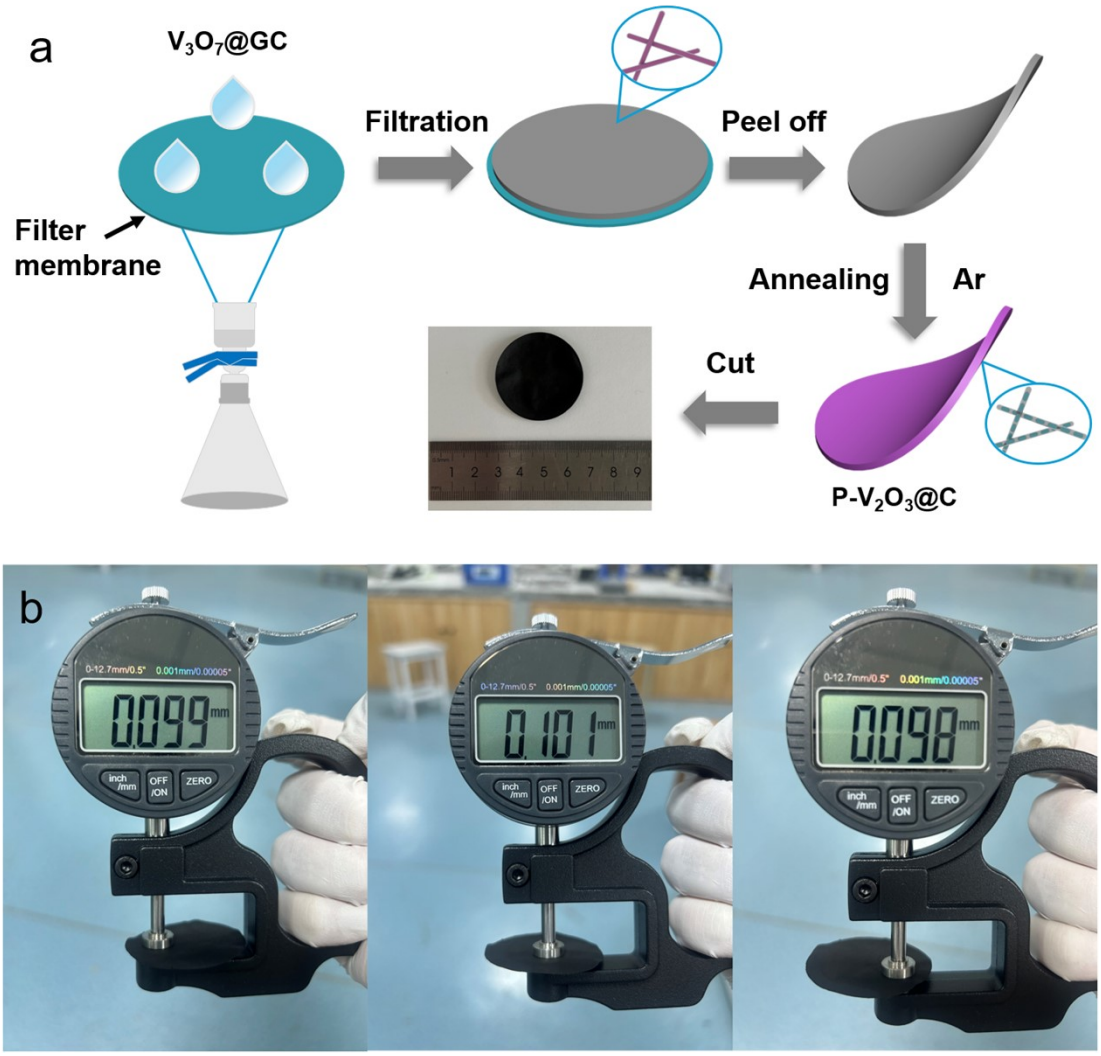

Fig. S2. (a)Schematic illustration of the fabrication of flexible and freestanding P-V_2O_3@C film electrode. (b) The thickness of the electrode was measured at different positions using a thickness gauge.

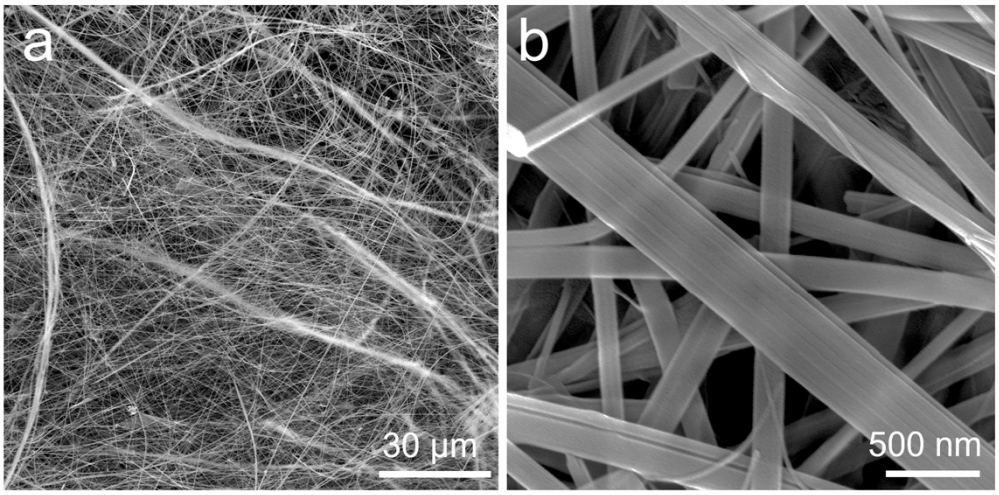

Fig. S3. SEM images of $V_3O_7 \cdot xH_2O$ nanowires.

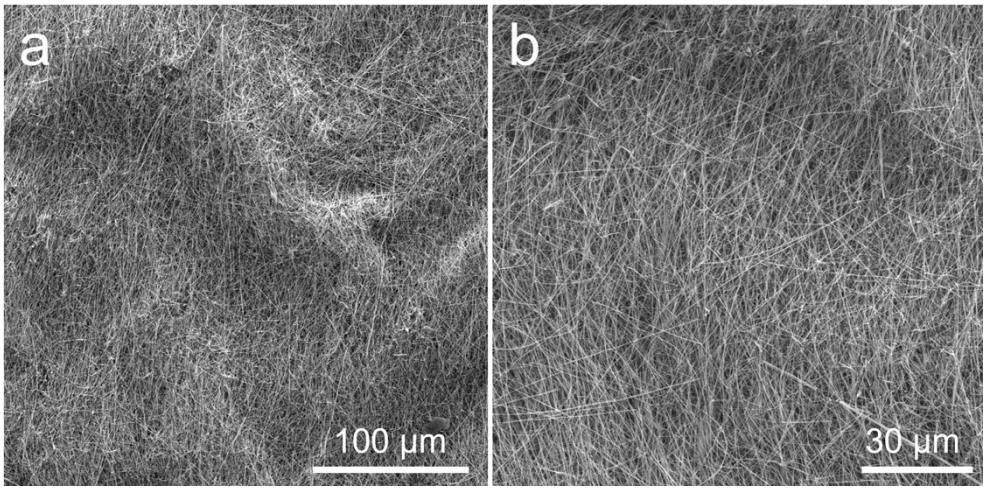

Fig. S4. SEM images of P-V_2O_3@C at low magnification.

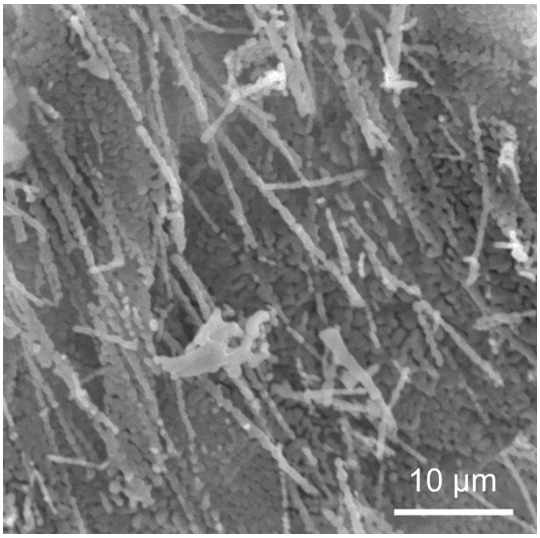

Fig. S5. SEM images of V_2O_3.

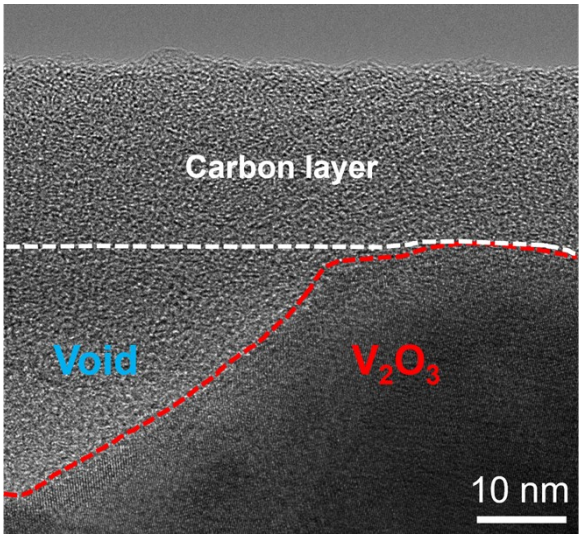

Fig. S6. TEM images of P-V_2O_3@C at high magnification.

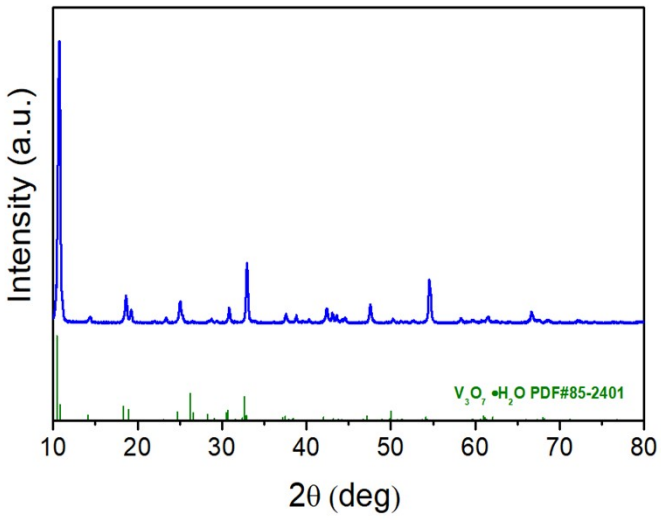

Fig. S7. XRD patterns of $V_3O_7 \cdot xH_2O$ nanowires.

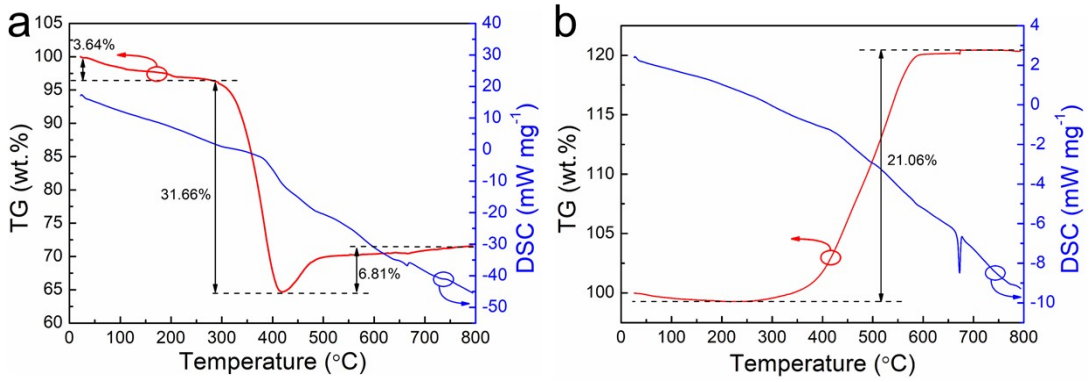

Fig. S8. TG-DSC curves of (a) P-V_2O_3@C and (b) V_2O_3.

$$V_2O_3(150) + O_2 = V_2O_5(182)$$

$$C + O_2 = CO_2$$

$$V_2O_3 = 71.51\% \times \frac{150}{182} = 58.94\%$$

$$V_2O_3 + C = 96.36\%$$

$$C = (96.36\% - 58.94\%)/96.36\% = 38.83\%$$

$$V_2O_3 = 58.94\%/96.36\% = 61.17\%$$

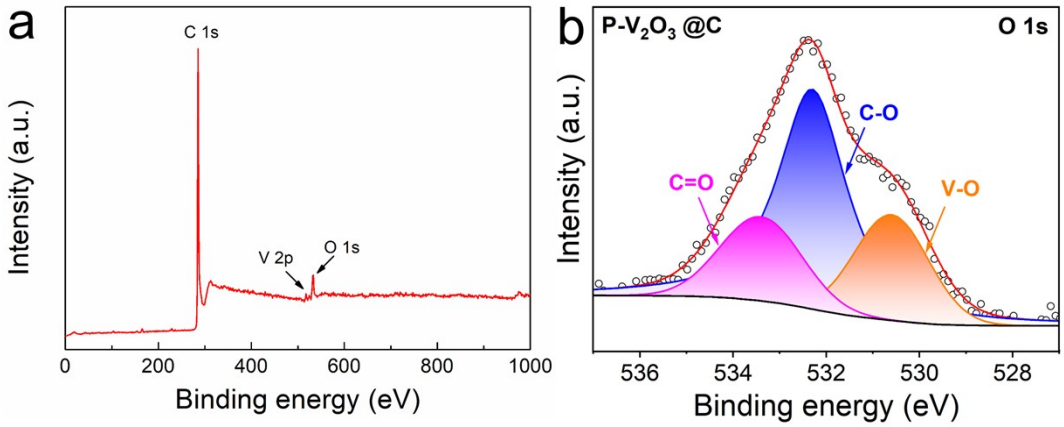

Fig. S9. (a) XPS survey spectra of P-V_2O_3@C and V 2p. (b) XPS fine spectra of O 1s.

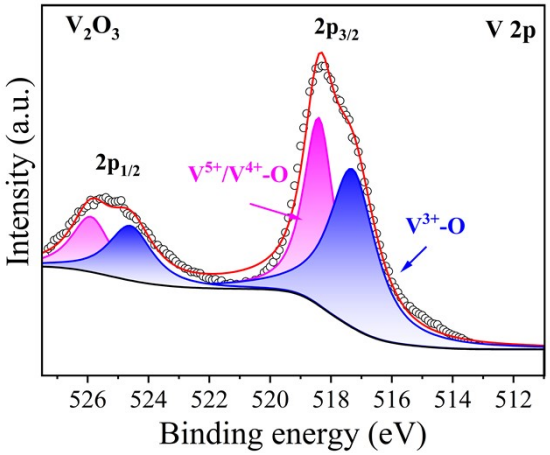

Fig. S10. XPS fine spectra of V 2p in pure V_2O_3.

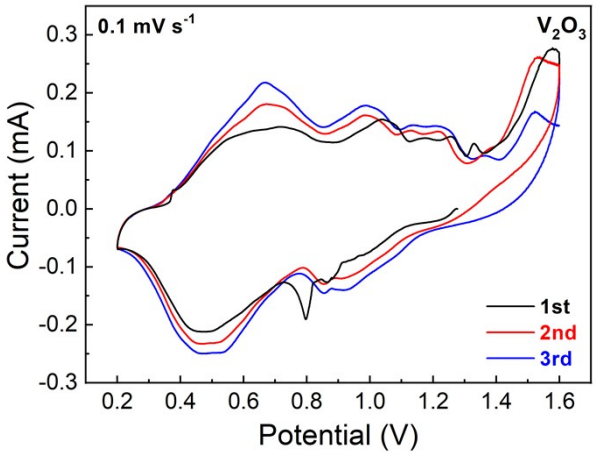

Fig. S11. CV curves of pure V_2O_3 at scan rates ranging from 0.1 mV s^{-1}.

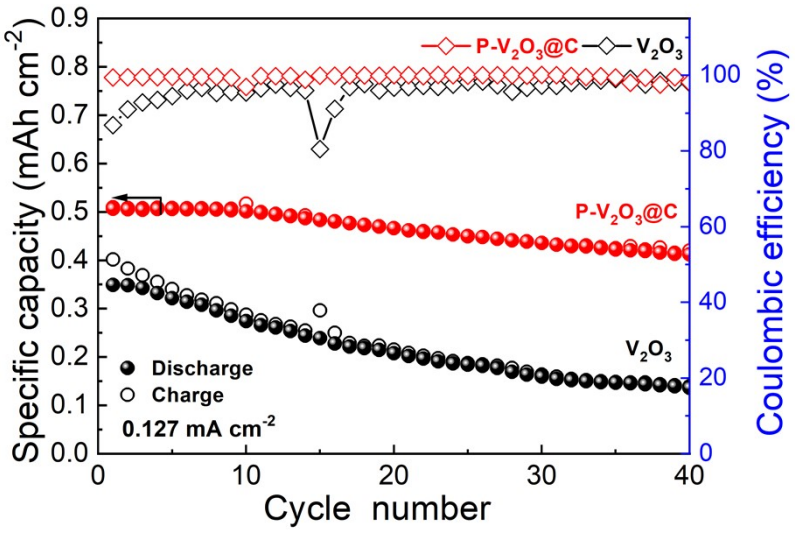

Fig. S12 Cycle performance of P-V_2O_3@C and V_2O_3 electrode at 0.127 mA cm^{-2}

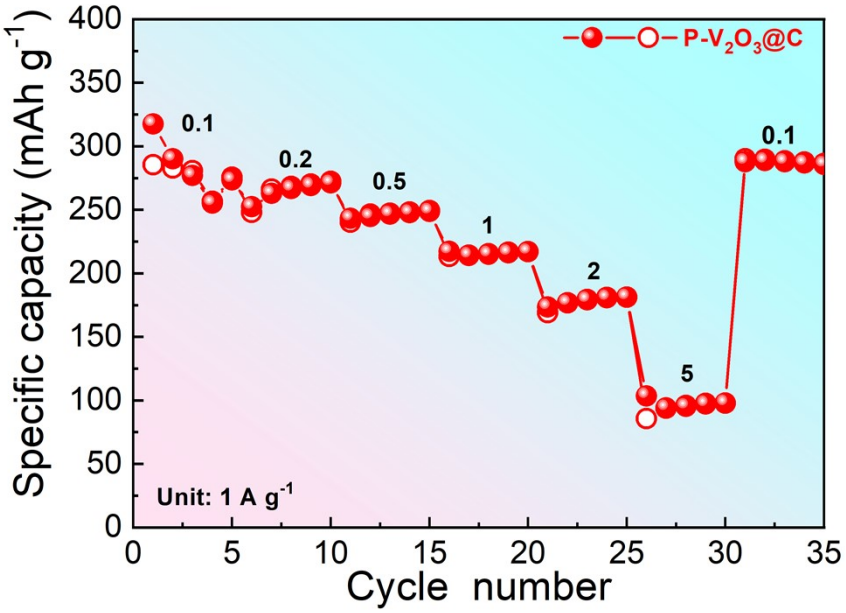

Fig. S13 Rate performance of P-V_2O_3@C thicker electrode (the mass loading is 3.5 mg cm^{-2}).

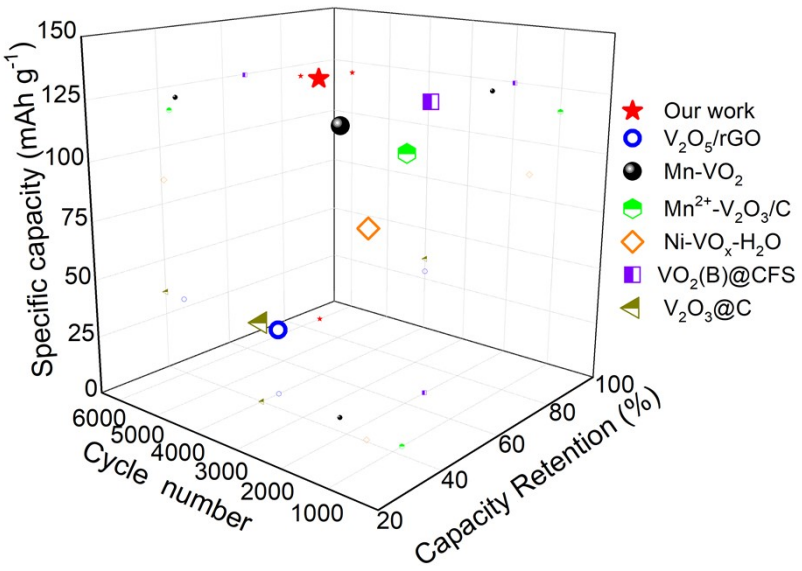

Fig. S14. The comparison of cycling behavior of P-V_2O_3@C cathode with reported V_xO_y-based cathodes at 5 A g^{-1} for AZIBs.

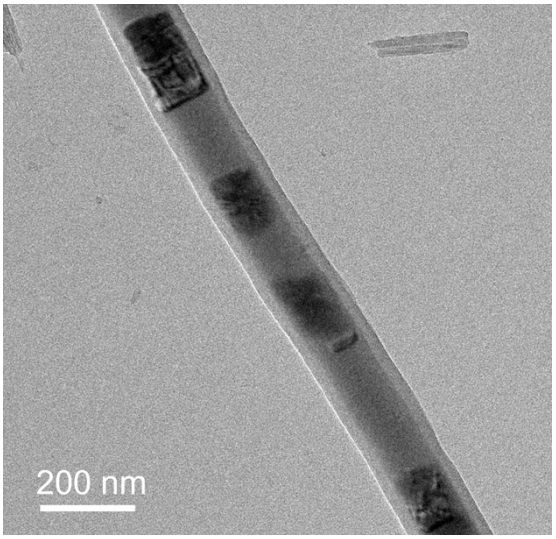

Fig. S15. TEM image of P-V_2O_3@C after long-term cycling

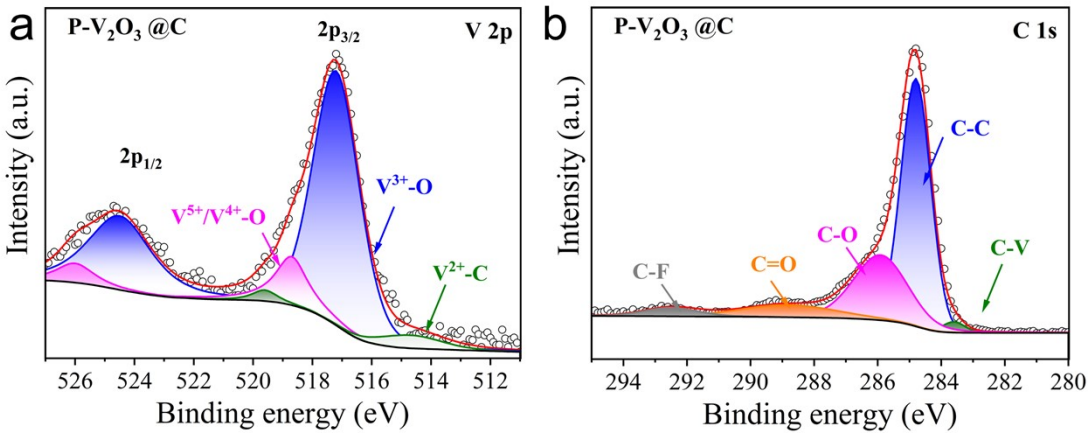

Fig. S16. XPS fine spectra of (a) V 2p and (b) C 1s in P-V_2O_3@C after long-term cycling.

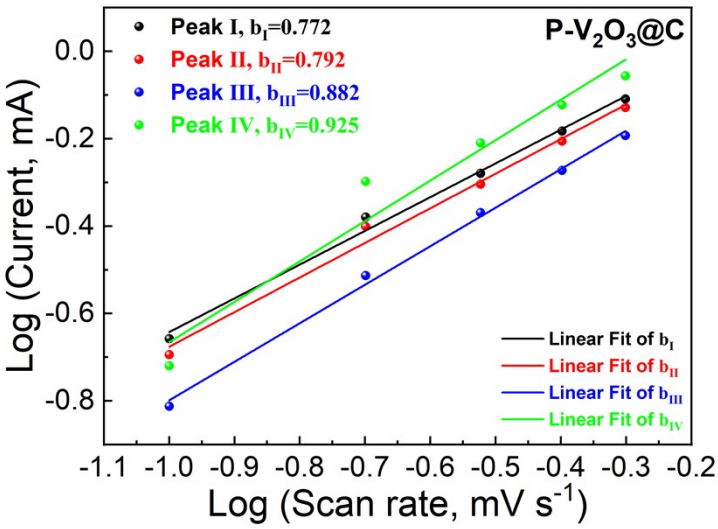

Fig. S17. Plots of the relationship between peak current and scan rates (log(*i*) vs log(*v*)) at each redox peak based on the CV curves.

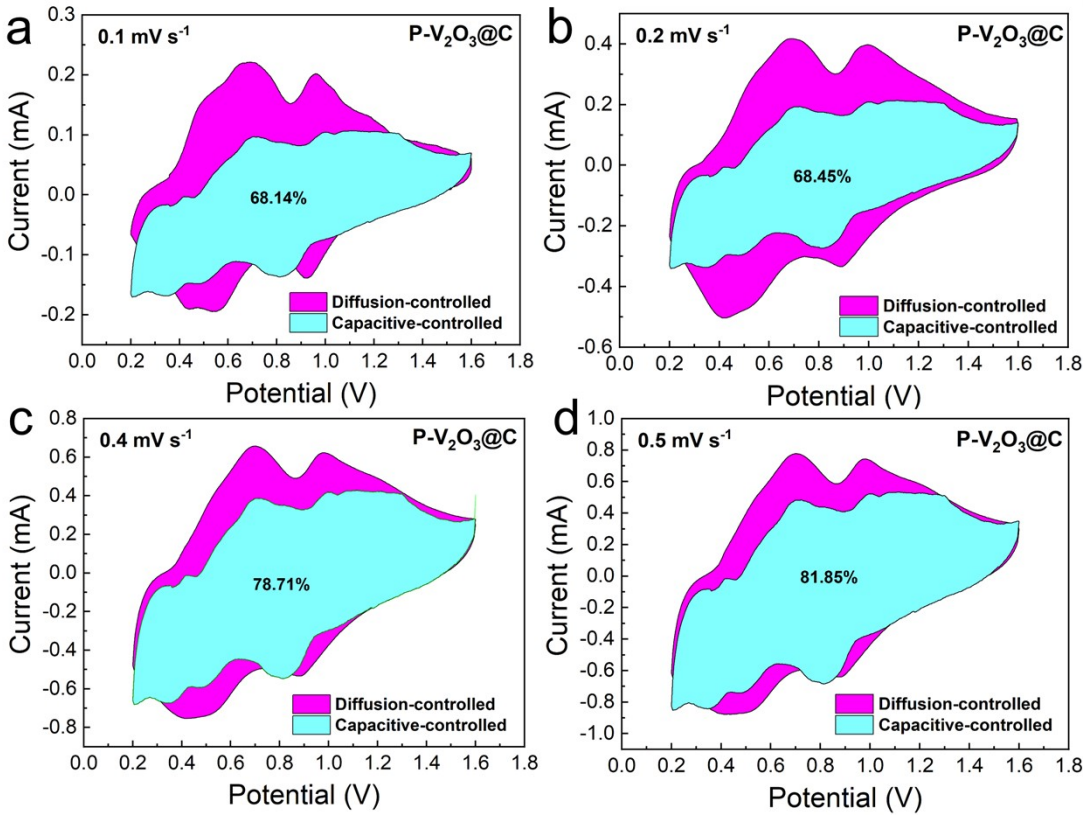

Fig. S18. CV curve and a capacitive contribution of P-V_2O_3@C at 0.1, 0.2, 0.4 and 0.5 mV s^{-1}.

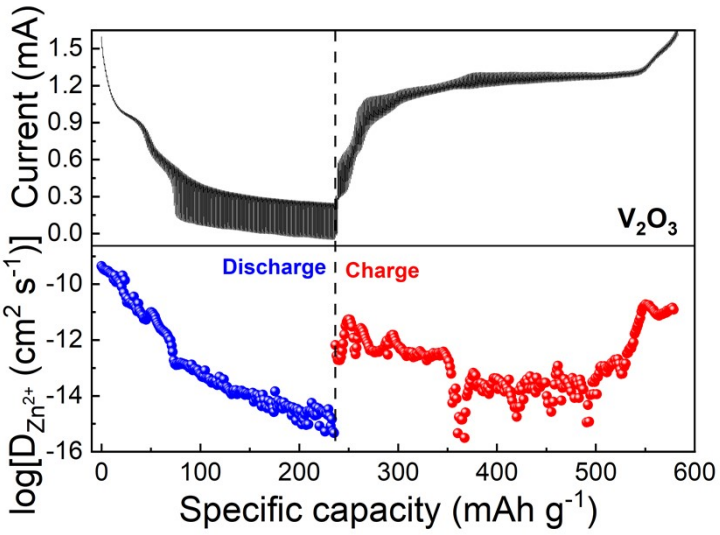

Fig. S19. Charge-discharge GITT curves of V_2O_3 at a current density of 20 mA g^{-1} and the corresponding Zn^{2+} diffusion coefficient (D_{Zn}^{2+}).

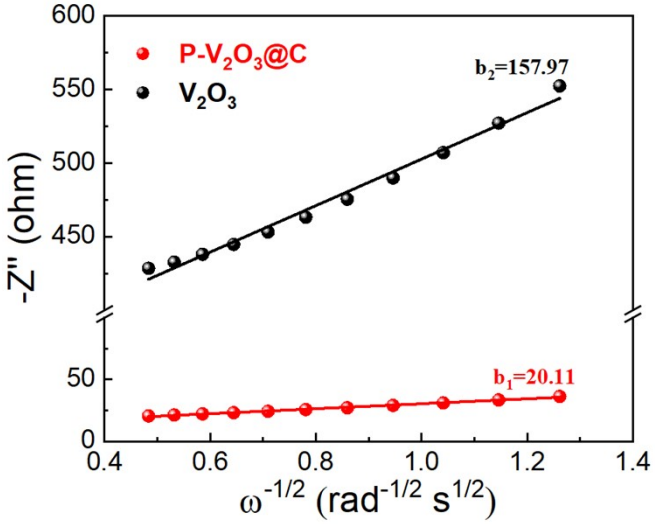

Fig. S20. Relationship between $\omega^{-1/2}$ and Z' in the low-frequency region.

The linear fit slope of P-V_2O_3@C (20.11 Ω $s^{-1/2}$) was lower than the values of pure V_2O_3 (157.97 Ω $s^{-1/2}$).

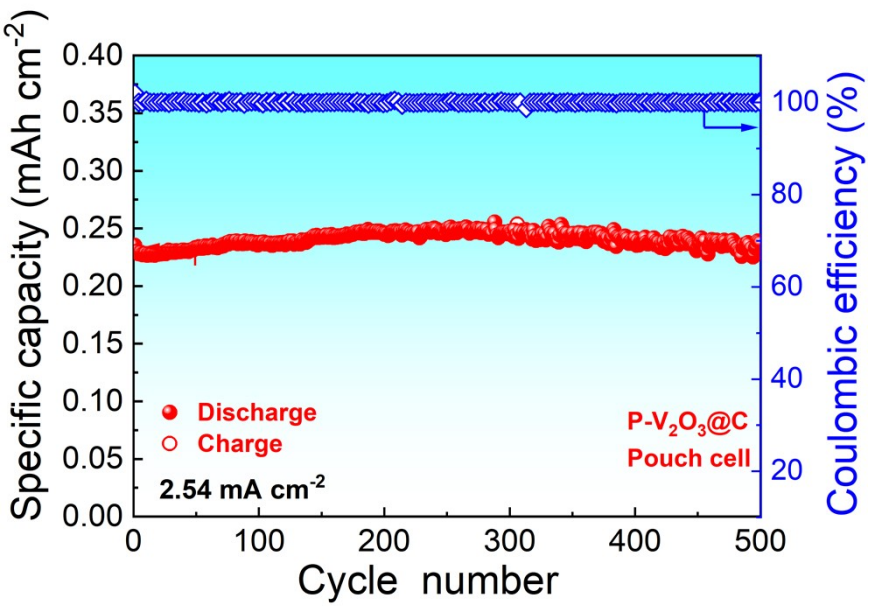

Fig. S21 Cycle performance of P-V_2O_3@C electrode for pouch cell at 2.54 mA cm^{-2}.

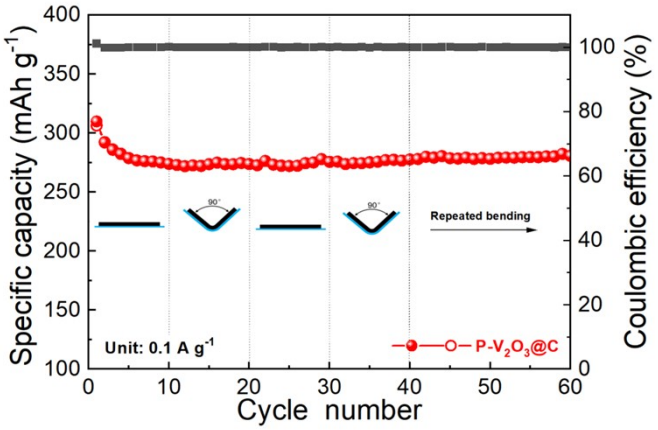

Fig. S22 Cycling performance under different bending states (0.1 A g^{-1}) of the P-V_2O_3@C-based flexible ZIBs.

Table S1. Fitted data from the electrochemical impedance spectra (EIS) of different samples.

Samples	R_0 **(Ω)**	R_{ct} **(Ω)**
P-V_2O_3@C	1.0	13.2
V_2O_3	1.9	213.7

Table S2. The comparison of cycling behavior of P-V_2O_3@C cathode with reported V_xO_y-based cathodes at 5 A g^{-1} for AZIBs.

Samples	**Specific capacity (mAh g^{-1})**	**Cycle number**	**Capacity Retention (%)**	**Ref.**
P-V_2O_3@C	**120**	**6000**	**87**	**our work**
V_2O_5/rGO	29	4000	46	[1]
Mn-VO_2	120	2500	45	[2]
Mn^{2+}-V_2O_3/C	115	1000	43	[3]
Ni-VO_x-H_2O	85	1600	41	[4]
VO_2(B)@CFS	125	2000	67	[5]
V_2O_3@C	35	4000	40	[6]

Table S3 The proportions of V^{5+}/V^{4+}-O, V^{3+}-O and V^{2+}-C in P-V_2O_3@C before and after cycling.

Samples	V^{5+}/V^{4+}-O (%)	V^{3+}-O (%)	V^{2+}-C (%)
P-V_2O_3@C	13.2	75.7	11.1
P-V_2O_3@C after cycling	14.6	78.5	6.9

References

1. X. Zheng, J. Tang, B. Ding, X. Hong, Q. Hu, Z. Liu, L. Zou, X. Zhou, P. Wang, C. Li and W. Nie, *Colloids Surf. Physicochem. Eng. Aspects*, 2024, **682**, 132864.
2. D. Wang, W. Liang, X. He, Y. Yang, S. Wang, J. Li, J. Wang and H. Jin, *ACS Appl. Mater. Interfaces*, 2023, **15**, 20876-20884.
3. C. L. Liu, Y. Liu, X. Liu and Y. Gong, *Sustain. Energ. Fuels*, 2022, **6**, 2020-2037.
4. J. Guo, J. Liu, W. Ma, Z. Sang, L. Yin, X. Zhang, H. Chen, J. Liang and D. a. Yang, *Adv. Funct. Mater.*, 2023, **33**, 2302659.
5. X. Li, L. Yang, H. Mi, H. Li, M. Zhang, A. Abliz, F. Zhao, S. Wang and H. Li, *CrystEngComm*, 2021, **23**, 8650-8659.
6. Y. Ding, Y. Peng, S. Chen, X. Zhang, Z. Li, L. Zhu, L.-E. Mo and L. Hu, *ACS Appl. Mater. Interfaces*, 2019, **11**, 44109-44117.